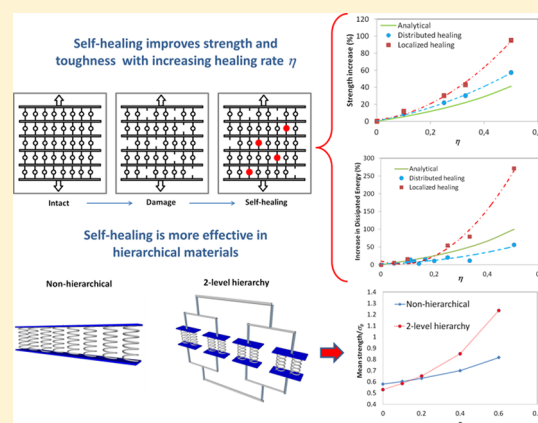


# Self-Healing of Hierarchical Materials

Federico Bosia,<sup>†</sup> Tamer Abdalrahman,<sup>‡</sup> and Nicola M. Pugno<sup>\*,§,||,⊥</sup><sup>†</sup>Department of Physics and “Nanostructured Interfaces and Surfaces” Centre, Università di Torino, Via P. Giuria 1, 10125 Torino, Italy<sup>‡</sup>Institute for Mechanics of Materials and Structures, Faculty of Civil Engineering, Vienna University of Technology, Karlsplatz 13/202, A-1040 Vienna, Austria<sup>§</sup>Laboratory of Bio-Inspired & Graphene Nanomechanics, Department of Civil, Environmental and Mechanical Engineering, Università di Trento, via Mesiano, 77, I-38123 Trento, Italy<sup>||</sup>Center for Materials and Microsystems, Fondazione Bruno Kessler, Via Sommarive 18, I-38123 Povo (Trento), Italy<sup>⊥</sup>School of Engineering and Materials Science, Queen Mary University of London, Mile End Road, London E1 4NS, United Kingdom

**ABSTRACT:** We present a theoretical and numerical analysis of the mechanical behavior of self-healing materials using an analytical model and numerical calculations both based on a Hierarchical Fiber Bundle Model, and applying them to graphene- or carbon-nanotube-based materials. The self-healing process can be described essentially through a single parameter, that is, the healing rate, but numerical simulations also highlight the influence of the location of the healing process on the overall strengthening and toughening of the material. The role of hierarchy is discussed, showing that full-scale hierarchical structures can in fact acquire more favorable properties than smaller, nonhierarchical ones through interaction with the self-healing process, thus inverting the common notion in fracture mechanics that specimen strength increases with decreasing size. Further, the study demonstrates that the developed analytical and numerical tools can be useful to develop strategies for the optimization of strength and toughness of synthetic bioinspired materials.



## 1. INTRODUCTION

One of the most fascinating bioinspired properties of materials, and thus far one of the least investigated, is that of self-healing (SH), that is, the property of a material to autonomically heal cracks, in other words to “repair itself”. This characteristic is drawn from nature where tissues like skin or bone are able to undergo long-term reparation after an instantaneous “trigger” or damaging event. Although the idea to try and replicate this behavior in artificial materials in itself is not new, its first successful realization dates to 2001, with the work of White et al.,<sup>1</sup> who embedded microcapsules containing a healing agent in a polymer composite, the cracking of which caused the healing agent to disperse, interact with catalysts, and polymerize in the composite. This concept was subsequently further developed to study fatigue life extension due to SH in the same system, obtaining up to 90% recovery of fracture toughness.<sup>2</sup> With this method, healing agent depletion leads to a reduction of SH in time, so that these types of materials have a limited “working life”. Chen and co-workers developed an organic polymeric material capable of healing by heating at above 120° and then recooling, with the advantage of not requiring a catalyst.<sup>3</sup> All of these approaches are well suited to stopping mainly macroscopic cracks, that is, catastrophic failure, but are scarcely effective in the case of distributed damage, as is common in fatigue experiments. “Vascular-based” SH systems were

accordingly developed to mimic blood circulation in the skin healing mechanism, thus avoiding healing agent depletion and enabling repeated healing. For example, a three-dimensional microvascular network was employed to deliver the healing agent to cracks in a polymer coating.<sup>4,5</sup> This technique allows repeated healing of the same crack, and has also been exploited to arrest and retard fatigue cracks.<sup>6</sup> Another approach to SH has been through so-called molecular-based systems. For example, Cordier et al. synthesized thermoreversible rubber that when broken or cut can be simply repaired by bringing together fractured surfaces to self-heal at room temperature.<sup>7</sup> Molecular-based systems have also been developed: Burnworth et al. demonstrated the synthesis of metallo-supramolecular polymers that heal when exposed to light,<sup>8</sup> and Chen et al. designed multiphase supramolecular thermoplastic elastomers that combine high modulus and toughness with spontaneous healing capability.<sup>9</sup> A comprehensive review of some of the most promising approaches to SH is given in ref 10.

Despite the great potential of the topic, relatively little has been done on the numerical modelization of SH. Most of the studies have concentrated on specific aspects of experiments,

Received: September 12, 2013

Revised: December 19, 2013

Published: December 23, 2013

for example, the modelization of the fracturing of the microcapsules containing the healing agent, and subsequent flow of the latter. For example, Verberg et al. used a hybrid approach with a coupled Lattice Boltzmann Model (LBM) and a Lattice Spring Model (LSM) to simulate the motion of microcapsules on a substrate with an adhesive coating under the effect of an imposed flow.<sup>11</sup> Maiti et al. studied the behavior of SH polymers applying coarse grained molecular dynamics on the atomistic scale in order to compute necessary parameters (e.g., local elastic modulus, reaction rates and cure kinetics) for the continuum macroscopic scale model.<sup>12</sup> Balazs and co-workers developed a hybrid computational approach using LSM and the Hierarchical Bell Model (HBM) to investigate the mechanical properties and SH behavior of nanogel particles connected by stable and labile bonds.<sup>13</sup> The combined LSM and modified HBM was also used to address the problem of designing strong and tough biomimetic polymer networks with the capability of reforming links in their chain.<sup>14</sup> A review of numerical methods applied to SH materials is given in ref 15. Despite the advances obtained through these studies, much remains to be done, and numerical modeling provides the means to minimize the cumbersome efforts in experimental work, optimizing the development of materials and highlighting the most relevant features of all tested solutions. In particular, since many macroscopic properties are a result of the behavior of the underlying nano- and microscale structures, a multiscale approach is essential to extract global physical and mechanical properties. In addition, due to the inherently hierarchical nature of natural materials, it is of great interest to evaluate the interaction of SH with hierarchical structure. The objective of this paper is thus to provide analytical and numerical tools to calculate multiscale mechanical properties of SH materials and discuss in particular the role of scaling, material structure and hierarchy. In particular, we apply these concepts to nanomaterials of great interest such as graphene or carbon nanotubes (CNTs), due to their particular relevance for the realization of bioinspired high-performance nanocomposites. Note that spontaneous healing mechanisms have been found at atomic level in CNTs through interaction with a metal catalyst<sup>16</sup> and in monatomic graphene sheets as a result of their interaction with metal impurities,<sup>17</sup> and new healing strategies can be conceived, for example, through the activation of carbon nanoscrolls.<sup>18</sup>

The paper is structured as follows: In section 2, an analytical formulation of the problem is discussed. In section 3, the numerical approach is presented. In section 4, calculation and simulation results are discussed, and numerical predictions are made for hierarchical structures. Finally, conclusions and an outlook are given.

## 2. SELF-HEALING HIERARCHICAL DANIEL'S THEORY

Many biological materials (e.g., cellular protein filaments, spider silk, tendon) display a fibrous structure, and several hierarchical levels can often be identified.<sup>19–21</sup> On the other hand, synthetic materials of interest for structural applications are often also fiber-based (e.g., graphene/CNT macroscopic fibers or graphene/CNT-reinforced composites), and hierarchy could be an important feature for future applications.<sup>22</sup> Therefore, to study the process of SH, we adopt a hierarchical fiber bundle model (HFBM) which extends the classical FBM, first introduced by Daniels<sup>23</sup> and extensively studied during the past years (see the review<sup>24</sup> and references therein). This model consists of arrays of fibers having statistically distributed strengths, arranged in parallel and in series to form hierarchical

architectures.<sup>28</sup> The “virtual” sample is loaded parallel to the fiber direction, and the fibers fail if the load exceeds their threshold value, with the load carried by the broken fiber being redistributed among the intact ones. This model is useful to simulate damage progression in a wide range of materials, not necessarily fibrous in structure.

**2.1. Engineering SH Parameter.** Here, we extend the approach proposed in ref 25 to hierarchical materials. For a large number  $N_0$  of fibers in a bundle, the number of surviving fibers  $N_{s0}$ , under an applied strain  $\epsilon$  and in the absence of SH, can be assumed to be

$$N_{s0} = N_0 \exp \left[ - \left( \frac{\epsilon}{\epsilon_0} \right)^m \right] \quad (1)$$

where  $\epsilon_0$  and  $m$  are the scale and shape parameters of the Weibull distribution for the fibers.<sup>26</sup> The fraction of broken fibers in the absence of SH is given by

$$\phi_0 = \frac{N_0 - N_{s0}}{N_0} \quad (2)$$

In the presence of SH, when the number of actual surviving fibers is  $N_{sh}$ , this becomes

$$\phi_h = \frac{N_0 - N_{sh}}{N_0} \quad (3)$$

We now introduce the parameter  $\lambda$  as the ratio between the number of broken fibers in the presence of SH and the number of broken fibers in the absence of SH:

$$\lambda = \frac{\phi_h}{\phi_0} = \frac{N_0 - N_{sh}}{N_0 - N_{s0}} \quad (4)$$

Finally, we introduce the healing parameter  $\eta$ , as

$$\eta = 1 - \lambda = \frac{N_{sh} - N_{s0}}{N_0 - N_{s0}} \quad (5)$$

so that  $0 < \eta < 1$ . If  $\eta = 0$ , we have  $N_{sh} = N_{s0}$  (no SH), whereas for  $\eta = 1$ ,  $N_{sh} = N_0$ ; that is, all fractured fibers heal. Since eqs 2 and 3 are reminiscent of the definition of engineering strain,  $\epsilon = (l - l_0)/l_0$ , we shall refer to  $\eta$  as “engineering SH parameter”.

**2.2. True SH Parameter.** We now introduce the “true” parameter  $\phi_h^*$  as

$$\phi_h^* = \int_{N_0}^{N_{sh}} \frac{dN}{N} = \ln N_{sh} - \ln N_0 = \ln \frac{N_{sh}}{N_0} \quad (6)$$

in analogy with the definition of true strain  $\epsilon = \int_{l_0}^l (dl/l) = \ln(l/l_0)$ . In the absence of SH, this becomes

$$\phi_0^* = \ln \frac{N_{s0}}{N_0} \quad (7)$$

So that the true SH parameter can be defined as

$$\eta^* = 1 - \lambda^* = 1 - \frac{\phi_{sh}^*}{\phi_0^*} = 1 - \ln \frac{N_{sh}/N_0}{N_{s0}/N_0} \quad (8)$$

The introduction of the true SH parameter in eq 8 is needed to take into account the variation of the total number of fibers induced by SH (similarly to the fact that true strain accounts for variations in the overall length  $l$ ). As can easily be verified, the parameters  $\eta$  and  $\eta^*$  coincide for  $N_{sh} \approx N_{s0} \approx N_0$ , that is, for relatively small damage levels. For simplicity, we will consider  $\eta$

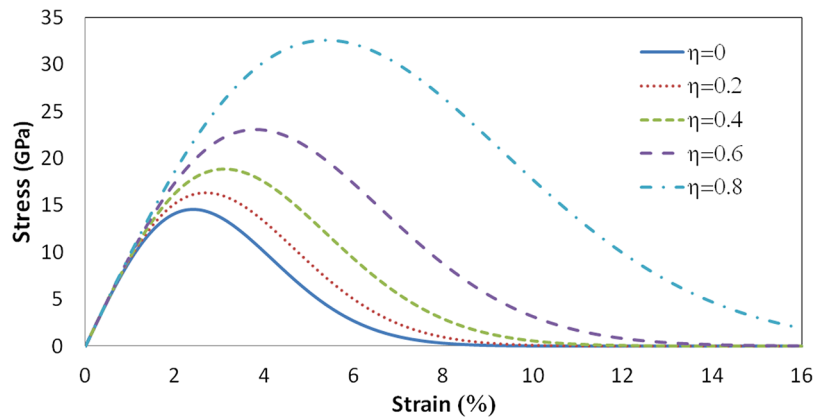


**Figure 1.** Analytically calculated stress–strain curves (in displacement control) for self-healing CNT-based specimens for various SH parameter values.

and  $\eta^*$  equivalent in the following. From eq 1, we immediately derive:

$$\ln \frac{N_{s0}}{N_0} = -\left(\frac{\varepsilon}{\varepsilon_0}\right)^m \quad (9)$$

By substituting eq 9 into eq 8, we find:

$$\ln \frac{N_{sh}}{N_0} = (\eta - 1) \left(\frac{\varepsilon}{\varepsilon_0}\right)^m \quad (10)$$

and thus

$$N_{sh} = N_0 \exp\left[(\eta - 1) \left(\frac{\varepsilon}{\varepsilon_0}\right)^m\right] \quad (11)$$

The introduction of SH into eq 11 generalizes the classical Weibull relation<sup>26</sup> which was used in eq 1. From eq 11, it is possible to derive the tensile stress  $\sigma$  corresponding to an applied strain  $\varepsilon$  as

$$\sigma(\varepsilon) = E\varepsilon \exp\left[(\eta - 1) \left(\frac{\varepsilon}{\varepsilon_0}\right)^m\right] = E_{eq}(\varepsilon, \eta)\varepsilon \quad (12)$$

where  $E$  is the single fiber Young's modulus. Thus, if the single fiber and bundle properties ( $E$ ,  $N_0$ ,  $m$ , and  $\varepsilon_0$ ) are known, stress–strain curves (in displacement control) can be calculated. Examples of these are shown in Figure 1 for  $N_0 = 5 \times 10^{10}$ ,  $E = 1$  TPa,  $\varepsilon_0 = 3.4\%$ , and  $m = 2$ , that is, typical parameters for CNTs (also similar to graphene nanoribbon characteristics). It is apparent that the bundle strength, ultimate strain, and toughness all increase with increasing healing parameter  $\eta$ . The mean strength  $\langle\sigma_D\rangle$  can be derived analytically from Daniels' theory<sup>23</sup> as

$$\langle\sigma_D\rangle = \frac{\varepsilon_0 E \exp(-1/m)}{[m(1 - \eta)]^{1/m}} \quad (13)$$

with standard deviation

$$\langle\theta_D\rangle = \sqrt{\frac{\langle\sigma_D\rangle^2 [1 - \exp(-1/m)]}{N_0 \exp(-1/m)}} \quad (14)$$

**2.3. Heterogeneous SH Materials.** Equation 12 can also be generalized to the case of a healing agent with different mechanical characteristics ( $E_2$ ,  $m_2$ , and  $\varepsilon_2$ ) from those of the original material ( $E_1$ ,  $m_1$ , and  $\varepsilon_1$ ), usually with  $\varepsilon_2 < \varepsilon_1$ . This

amounts to modeling a heterogeneous material, as discussed in,<sup>27</sup> with the percentage of the two phases varying with strain, and therefore damage level. Let us suppose that the specimen is made up initially only of type 1 fibers and that it heals only with type 2 fibers. The variation of the number of fibers of type 2 is described by eq 11, but instead of a constant initial number of fibers  $N_0$ , the exponential part must multiply the number of broken type 1 fibers (i.e.,  $N_0 - N_0 \exp[-(\varepsilon/\varepsilon_1)^{m_1}]$ ), multiplied by the healing parameter  $\eta$ . Thus:

$$N_{sh} = N_0 \exp\left[-\left(\frac{\varepsilon}{\varepsilon_1}\right)^{m_1}\right] + \eta N_0 \left\{1 - \exp\left[-\left(\frac{\varepsilon}{\varepsilon_1}\right)^{m_1}\right]\right\} \times \left\{\exp\left[(\eta - 1) \left(\frac{\varepsilon}{\varepsilon_2}\right)^{m_2}\right] - \exp\left[-\left(\frac{\varepsilon}{\varepsilon_2}\right)^{m_2}\right]\right\} \quad (15)$$

Since from eq 5  $\eta$  can be rewritten as  $\eta = (N_{sh} - N_{s0}^{(2)}) / (N_0 - N_{s0}^{(1)})$ , where the superscript indicates the fiber type and  $N_{s0}^{(2)}(t = 0) = 0$ , we have

$$\eta = \frac{\exp\left[(\eta - 1) \left(\frac{\varepsilon}{\varepsilon_1}\right)^{m_1}\right]}{1 - \exp\left[-\left(\frac{\varepsilon}{\varepsilon_1}\right)^{m_1}\right]} \quad (16)$$

and thus

$$N_{sh} = N_0 \exp\left[-\left(\frac{\varepsilon}{\varepsilon_1}\right)^{m_1}\right] + N_0 \left\{\exp\left[(\eta - 1) \left(\frac{\varepsilon}{\varepsilon_1}\right)^{m_1}\right]\right\} \times \left\{\exp\left[(\eta - 1) \left(\frac{\varepsilon}{\varepsilon_2}\right)^{m_2}\right] - \exp\left[-\left(\frac{\varepsilon}{\varepsilon_2}\right)^{m_2}\right]\right\} \quad (17)$$

and finally

$$\sigma = \varepsilon \left\{E_1 \exp\left[-\left(\frac{\varepsilon}{\varepsilon_1}\right)^{m_1}\right] + E_2 \left\{\exp\left[(\eta - 1) \left(\frac{\varepsilon}{\varepsilon_1}\right)^{m_1}\right]\right\} \times \left\{\exp\left[(\eta - 1) \left(\frac{\varepsilon}{\varepsilon_2}\right)^{m_2}\right] - \exp\left[-\left(\frac{\varepsilon}{\varepsilon_2}\right)^{m_2}\right]\right\}\right\} \quad (18)$$

This equation provides the correct limiting behavior:

$$\text{for } \eta = 0: \quad N_{\text{sh}} = N_{s0} = N_0 \exp\left[-\left(\frac{\varepsilon}{\varepsilon_1}\right)^{m_1}\right] \quad (19)$$

for  $\eta = 1$ :

$$N_{\text{sh}} = N_0 \exp\left[-\left(\frac{\varepsilon}{\varepsilon_1}\right)^{m_1}\right] + N_0 \left\{1 - \exp\left[-\left(\frac{\varepsilon}{\varepsilon_2}\right)^{m_2}\right]\right\} \quad (20)$$

which both for  $\varepsilon = 0$  and for  $\varepsilon \rightarrow \infty$  gives  $N_{\text{sh}} = N_0$ .

**2.4. Hierarchical SH.** Finally, we consider the effect of SH in hierarchical materials. We adopt the procedure outlined in ref 28, whereby the Weibull parameters at hierarchical level  $n$  are derived from those at hierarchical level  $(n - 1)$  using Daniels' theory.<sup>23</sup> For example, based on eq 11, the Weibull distribution at the first hierarchical level can be taken to be

$$W(\varepsilon) = 1 - \exp\left[(\eta - 1)\left(\frac{\varepsilon}{\varepsilon_{h1}}\right)^{m_{h1}}\right] \quad (21)$$

with  $\varepsilon^{(1)}$  and  $m^{(1)}$  being the unknown scale and shape parameters at level 1. The mean strength and standard deviation of this distribution are

$$\langle\sigma_{Wh1}\rangle = \frac{E\varepsilon_{h1}}{(1 - \eta)^{1/m_{h1}}}\Gamma\left(1 + \frac{1}{m_{h1}}\right) \quad (22)$$

and

$$\theta_{Wh1} = \langle\sigma_{Wh1}\rangle \sqrt{\frac{\Gamma\left(1 + \frac{2}{m_{h1}}\right)}{\Gamma^2\left(1 + \frac{1}{m_{h1}}\right)} - 1} \quad (23)$$

By setting  $\langle\sigma_{Wh1}\rangle$  and  $\theta_{Wh1}$  equal to the mean strength and standard deviation obtained at level 0 through eqs 13 and 14, it is possible to derive  $\varepsilon_{h1}$  and  $m_{h1}$ .<sup>28</sup> By repeating this procedure iteratively up to level  $n$ , the Weibull parameters  $\varepsilon_{h(n+1)}$  and  $m_{h(n+1)}$  at any hierarchical level  $n + 1$  can also be obtained from those at level  $n$  ( $\varepsilon_{hn}$  and  $m_{hn}$ ), by numerically solving the two following coupled equations:

$$\frac{\varepsilon_{h(n+1)}}{(1 - \eta)^{1/m_{h(n+1)}}}\Gamma\left(1 + \frac{1}{m_{h(n+1)}}\right) = \frac{\varepsilon_{hn} \exp(-1/m_{hn})}{[m_{hn}(1 - \eta)]^{1/m_{hn}}} \quad (24)$$

$$\frac{\Gamma\left(1 + \frac{2}{m_{h(n+1)}}\right)}{\Gamma^2\left(1 + \frac{1}{m_{h(n+1)}}\right)} = \frac{1 - \exp(-1/m_{hn})}{N_n \exp(-1/m_{hn})} + 1 \quad (25)$$

The effect of SH occurring at different hierarchical levels can therefore be evaluated, and the corresponding strength of different hierarchical structures can be calculated.

### 3. NUMERICAL SELF-HEALING HIERARCHICAL FIBER BUNDLE MODEL

Though some interesting features of SH can be derived analytically, as discussed in the previous section, it is necessary to resort to numerical FBM simulations to additionally derive more advanced features. In previous work, we have developed a recursive, or "hierarchical", formulation of a FBM, which we have called HFBM,<sup>29</sup> and which has been used to study

multiscale problems ranging from nanoscale to macroscale<sup>28,30</sup> and composite materials with mixed brittle-ductile properties.<sup>31</sup> The multilevel scheme is implemented by formulating the problem at all relevant size scales using various ( $n$ ) hierarchical levels and recursively deriving level  $(n + 1)$  fiber characteristics like strength, toughness, and Young's modulus, from level  $n$  simulations.<sup>30</sup> This model has recently been applied to heterogeneous materials, constituted of fibers with different mechanical characteristics, to determine the influence of hierarchy and material mixing in the optimization of the global material properties.<sup>27</sup> In spite of its simplicity, the HFBM can capture many important aspects of damage phenomena in heterostructured materials, and SH can be easily included in the model. This can be done by replacing fractured fibers with intact ones having appropriate mechanical properties, volume fractions, replacement rates and locations as damage evolves during simulations. This is schematically shown in Figure 2a.

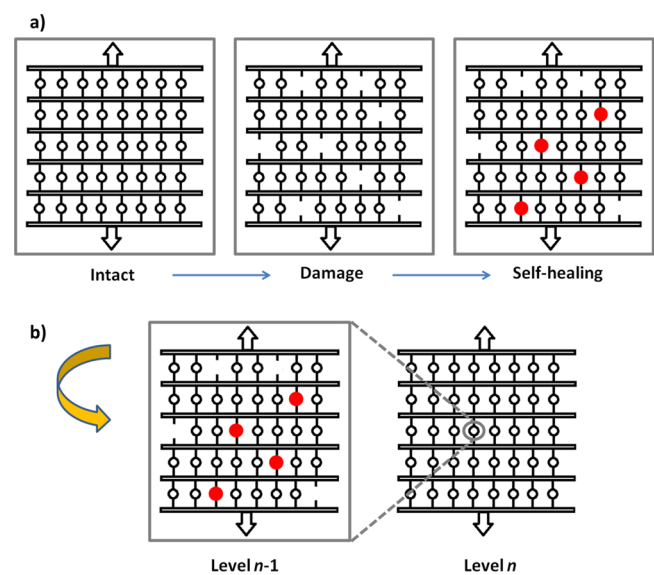


**Figure 2.** (a) Schematic representation of damage/SH process in a fiber bundle. Broken fibers are represented by missing circles, and healed fibers are represented by filled circles. The healing rate is  $\eta = 0.5$ , so that half of the damaged fibers are replaced by healed fibers; (b) hierarchical implementation of the fiber bundle model: level  $n$  properties are derived from repeated simulations at level  $(n - 1)$ .

The multiscale hierarchical scheme can be applied in this case too, by calculating level  $n$  single fiber properties from repeated simulations on level  $(n - 1)$  bundles, as shown in Figure 2b. Thus, the simulations can account for SH at any given hierarchical level, providing useful information about the scaling of material properties with size, and the effectiveness of SH at each hierarchical scale.

In this case, the control parameter is the so-called "healing rate"  $\gamma$ , defined as the ratio between the number of "healed fibers"  $N_h$  and the number of fractured fibers  $N_f$  in a given fixed time interval. Since  $N_{\text{sh}} = N_0 - N_f + N_h$  and  $N_{s0} = N_0 - N_f$ , the definition of  $\gamma$  coincides with that of  $\eta$  introduced in section 2:

$$\gamma = \frac{N_h}{N_f} = \frac{N_{\text{sh}} - N_{s0}}{N_0 - N_{s0}} = \eta \quad (26)$$

In the following, results will be presented as a function of  $\eta$ . Contrary to the analytical treatment of the problem, in the numerical case it is possible to control another critical

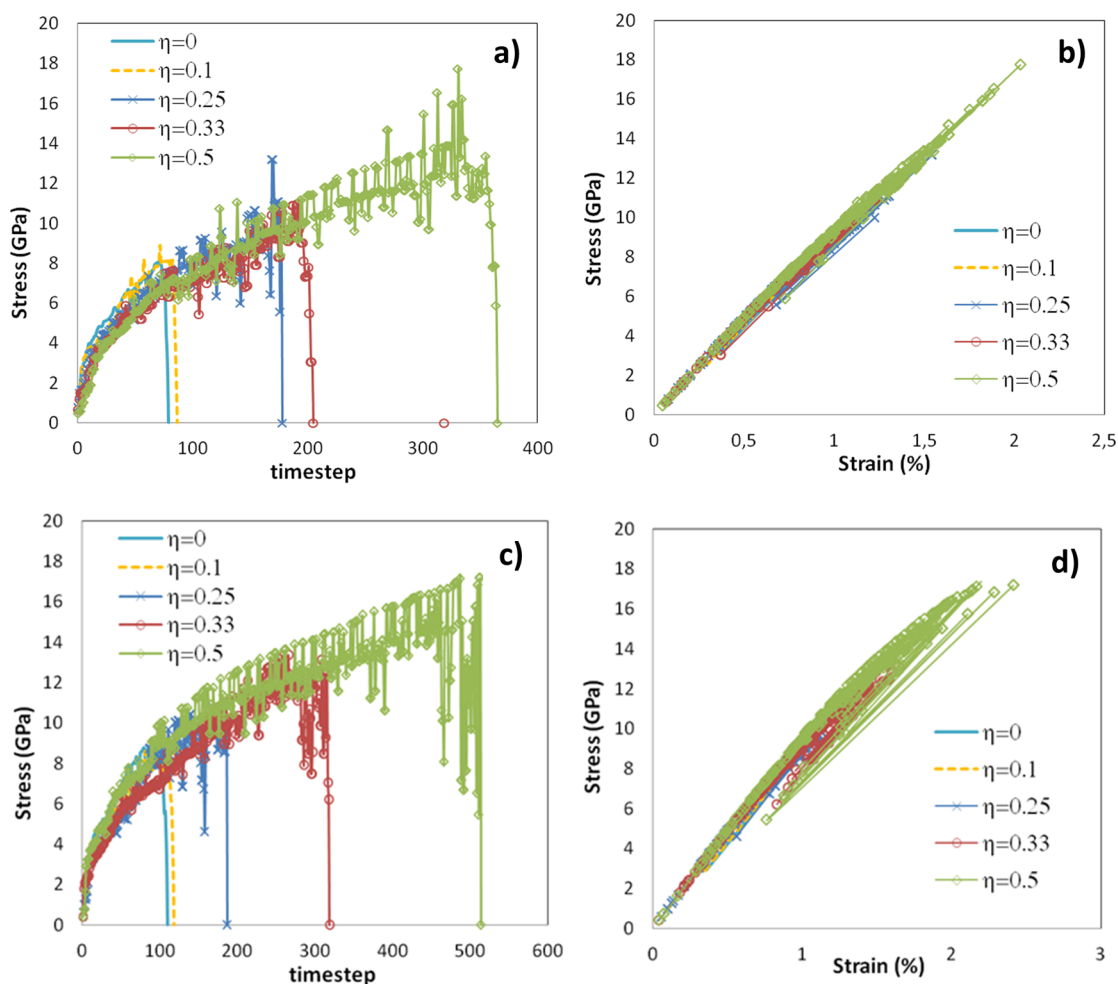


**Figure 3.** (a) Time evolution of stress in SH specimens subjected to traction up to rupture for various healing rates ( $\eta = 0.1, 0.25, 0.33, 0.5$ ), in distributed healing configuration. (b) Stress vs strain behavior in distributed healing configuration. (c) Stress vs time in local healing configuration. (d) Stress vs strain behavior (all simulations in crack-opening displacement control).

simulation parameter, which is the location where fibers are reintroduced. In the present study, two different scenarios are considered: (a) Distributed healing: Fibers are reintroduced at a random locations in the fiber bundle where fibers have previously fractured. (b) Local healing: Fibers are reintroduced at the location of the last fractured fiber. These two modeling situations correspond, roughly speaking, to two limiting cases in which the effectiveness of SH is (a) minimized and (b) maximized, respectively, with distributed material damage in the first case (i.e., uniformly distributed microcracking), or macroscopic cracking in the second.

## 4. NUMERICAL VERSUS THEORETICAL RESULTS

**4.1. Homogeneous Material-Healing Agent Properties.** First, we perform numerical simulations and consider the case in which the mechanical characteristics of the healing agent are identical to those of the host material. This means that when healing occurs, fractured fibers in the bundle are replaced by fibers with statistically equivalent mechanical characteristics. We use the same CNT material properties as above for the single fiber type involved in the simulations: Young's modulus  $E = 1$  TPa, Weibull shape parameter  $m = 2$ , and Weibull scale parameter  $\epsilon_0 = 3.4\%$ .

Various healing rates are analyzed to begin with, ranging from  $\eta = 0.1$  to  $\eta = 0.5$ , and both distributed and local healing

are considered. Simulations are carried out in crack-opening displacement control instead of displacement or load control, in order to monitor damage evolution for every fiber-break.

A typical example of the stress evolution in a specimen subjected to uniaxial tensile loading is shown in Figure 3a, in the case of distributed healing. The oscillating behavior in the numerical curves is due to the alternating fiber ruptures and healing events. The effect of increasing healing rate is evident in the data. Stress strain curves (Figure 3b) display only minimal softening before specimen failure, indicating SH in this case does not modify the brittle material behavior. Here, the crack-opening displacement control of the numerical test is responsible for the simultaneous decrease of both stress and strain after fiber rupturing.

In the local healing configuration, the time evolution of stress curves up to specimen failure shows a longer time-to-failure (Figure 3c), although the strength remains similar to the distributed healing case (Figure 3d). This fact highlights the greater effectiveness of local healing, for equivalent healing rates, in ensuring structural integrity of the material. Also, stress-strain curves display some softening before failure for high  $\eta$  values.

This observation is confirmed by further analysis on the simulation data. For example, Figure 4a and b illustrates the failure strength distributions obtained in repeated simulations

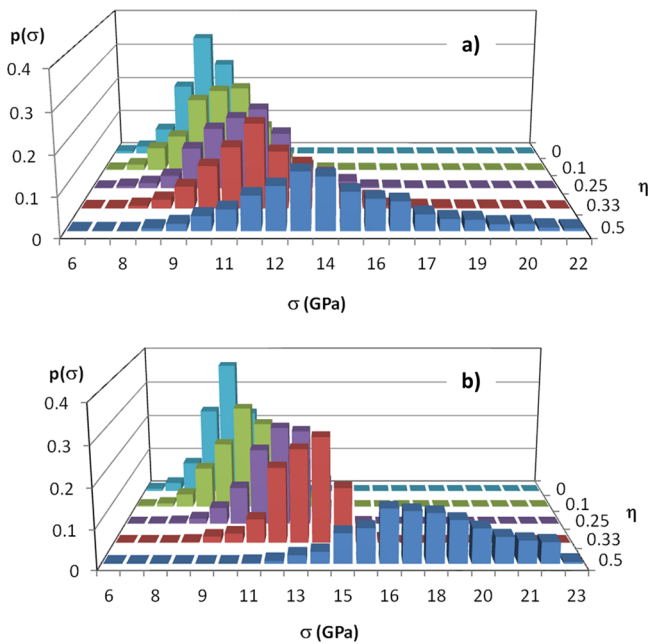


**Figure 4.** Strength distributions for (a) distributed healing and (b) local healing, with  $\eta = 0, 0.1, 0.25, 0.33, 0.5$ .

on specimens in distributed and local healing configurations, respectively. It is apparent that the mean strength increases monotonically with healing rate, as does the dispersion of the distributions. Looking at mean strength values, the effect of SH is to cause the material strength to increase by up to 57% in the case of distributed healing (from 8.8 GPa in the absence of healing to 13.9 GPa for  $\eta = 0.5$ ), and by 95% in the case of local healing (from 8.8 to 17.2 GPa for  $\eta = 0.5$ ). These data are compared to analytical results in Figure 5a. The latter slightly underestimate numerical values, probably due to the simplified analytical approach. Energetic aspects of material damage can also be considered using both the analytical approach and the HFBM. The dissipated energy in the formation of a crack surface at micro- or mesoscale is estimated by performing integration of the resulting stress–strain curves obtained analytically and numerically. Results are shown in Figure 5b. Here, while the distributed healing configuration can increase dissipated energy, and hence the material toughness, by up to 50% for  $\eta = 0.5$ , the improvement reaches 270% in the case of local healing for  $\eta = 0.5$ . This indicates that SH can bring about considerable strength enhancements, but even more so toughness improvements. Analytical results do not underestimate numerical values in this case, probably due to the fact that stress–strain curves are analytically calculated in displacement control, while numerical curves are obtained in crack-opening displacement control, so that the underlying areas are smaller in the numerical case. It is interesting to note that all curves in Figure 5a and 5b display a nonlinear dependence with respect to  $\eta$  and are approximately quadratic in all cases.

Another important effect of SH is the influence on the time to failure for specimens tested in crack-opening control. Using the HFBM, it is also possible to estimate this quantity as a function of SH rate. This is shown in Figure 5c. In this case, no analytically calculated values are reported, as they would not be comparable to the numerically derived values, due to the different adopted loading control configurations. The same increasing tendency is highlighted as in Figure 5a and b, with a

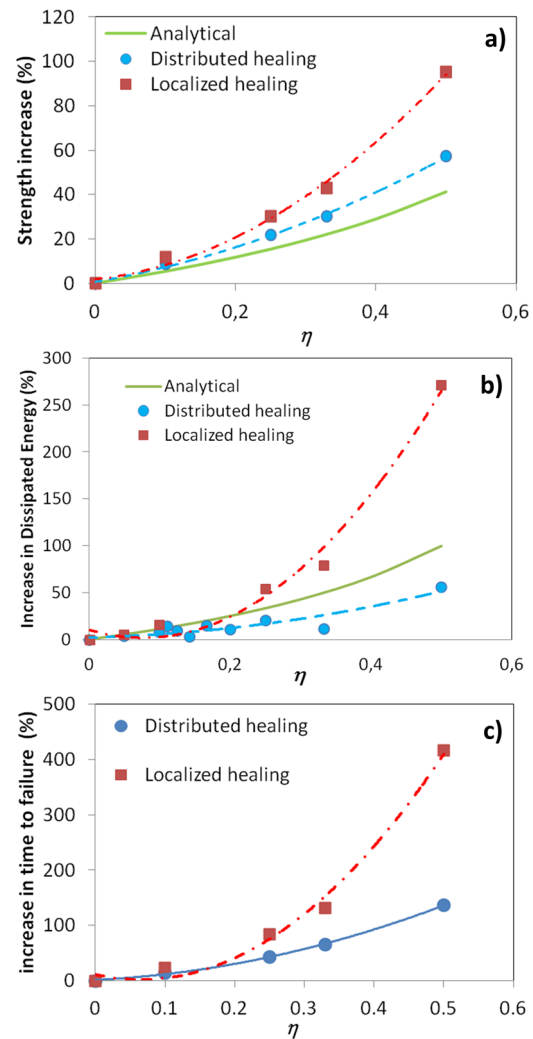


**Figure 5.** Calculated and simulated variations in (a) mean strength and (b) dissipated energy as a function of healing rate  $\eta$  in the case of distributed and local SH. (c) Simulated time to failure as a function of  $\eta$  in the case of distributed and local SH. Quadratic fits on all numerical data are included.

maximum increase in time to failure of 136% and 416% for  $\eta = 0.5$  and distributed and local healing, respectively. These values prove how the use of SH can improve material properties considerably, especially in the case of local healing, and simulations can be extended to fatigue experiments to predict improved specimen lifetimes.

**4.2. Heterogeneous Material-Healing Agent Properties.** Next, we consider a condition which potentially occurs experimentally, when the healing agent often displays considerably reduced mechanical properties with respect to the original material. In this case, it is reasonable to expect reduced SH efficiency in recovering mechanical properties. Numerical simulations can help in this case in quantifying the effect. We thus consider the following mechanical properties for the healing agent Young's modulus  $E_h = E_t/5 = 200$  GPa and Weibull scale parameters  $\epsilon_h = 0.04$ ,  $m_h = 1.5$ , and carry out simulations for a biphasic material corresponding to the ideal case of a graphene/CNT-based material with a healing agent with reduced mechanical properties. Results are discussed for a distributed healing configuration only, as this corresponds to the situation that best corresponds to the analytical model. As

shown in Figure 6, analytical and numerical results are in good agreement, despite the simplifications discussed above. Here,

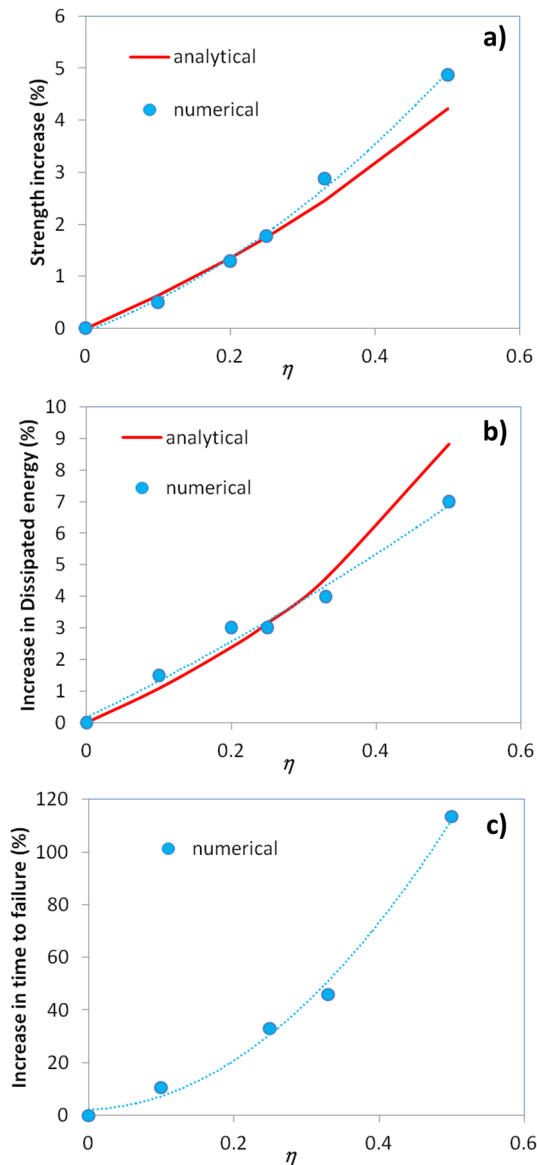


**Figure 6.** Calculated and simulated variations in (a) mean strength, (b) dissipated energy, and (c) time to failure as a function of healing rate  $\eta$  in the case of a healing agent with reduced mechanical properties with respect to the host material (numerical results are relative to distributed SH).

the effect of SH on strength and toughness is strongly reduced, and the approximately 5-fold reduction in healing agent stiffness and strength results in an even greater reduction in the effect of SH on strength (only a 5% strength increase compared to the previous 56% for  $\eta = 0.5$ ). The reduction is smaller in the case of toughness, with an approximate increase in dissipated energy of 7–9% instead of 39%. On the other hand, the effect on the time-to-failure remains considerable, with a 114% increase compared to the previous 416% for  $\eta = 0.5$  (only numerical results are considered here). This shows that healing agent mechanical properties are an important factor to consider in the design of efficient SH materials: it is essential to obtain mechanical properties as close as possible to

those of the host material, if not superior, to maximize the effectiveness of the SH process.

Results from numerical simulations in a local healing configuration are summarized in a wider parameter range in Figure 7, where property maps are provided as a function of varying healing agent stiffness  $E_h$  and strength  $\sigma_h$ , as well as healing parameter  $\eta$ . Figure 7a shows the overall strength improvement as a function of  $\sigma_h/\sigma_f$  and  $\eta$ , Figure 7b the overall increase in dissipated energy (in log scale) as a function of  $\sigma_h/\sigma_f$  and  $\eta$ , Figure 7c the overall strength improvement (in log scale) as a function of  $E_h/E_f$  and  $\eta$ , and Figure 7d the overall increase in dissipated energy (in log scale) as a function of  $E_h/E_f$  and  $\eta$ . Some irregularities in the patterns of the maps appear, due to the statistical nature of the simulations. These maps could provide useful information for the design of experimental studies, once relevant material properties are known.

**4.3. SH in Hierarchical Structures.** Next, the effect of SH on a hierarchical structure is evaluated by using the HFBM, that is, by applying the FBM recursively, as explained in section 3, and comparing results to analytical calculations using the hierarchical procedure described in section 2.4. Since analytical results have been seen to be representative of a distributed healing configuration, only this configuration is considered in numerical simulations. Each hierarchical level corresponds to a different size scale, depending on the chosen modeling parameters (number of fibers in series and in parallel). As an example, we consider a 4-level hierarchical structure ranging from a length of 100 nm (fiber dimension at level 1) to 1 mm at level 4. For brevity, we only analyze specimen strength to evaluate effectiveness of SH. First, we consider the case in which SH occurs at the same rate at all hierarchical levels, using a healing agent with the same mechanical properties as the original material (i.e., those specified at the beginning of section 4). The assumption here is that SH can occur at various size scales in an equivalent manner, i.e. it can be triggered by micro-to macrocracks. Clearly, this ideal case is a simplification, but it serves the purpose of determining a benchmark with which to compare more realistic scenarios. Analytical and numerical results for this case are shown in Figure 8a, where the ratios between the strength and the level-0 Weibull scale parameter are plotted for various healing ratios. The decreasing trend with increasing hierarchical level is consistent with previous results obtained for homogeneous materials,<sup>27</sup> but it is apparent that SH introduces significant improvements to the mean strength at all hierarchical levels. There is some discrepancy between analytic and numerical results, possibly highlighting the need for appropriate correction factors in the analytical hierarchical formulation, as discussed in ref 28.

The exploitation of healing agents with superior mechanical properties with respect to the host material provides, at least theoretically, the possibility of reversing the trend shown in Figure 8a, that is, decreasing strength for increasing hierarchical levels. One numerically calculated example is shown in Figure 8b, where data are reported for a healing agent 100 times stiffer and stronger than the host material:  $E_h = 100E_f$ ,  $\sigma_h = 100\sigma_f$ . To obtain an increase in strength with each hierarchical level, the healing rates are suitably graded at each level:  $\eta_1 = 0$ ,  $\eta_2 = 0.11$ ,  $\eta_3 = 0.17$ ,  $\eta_4 = 0.25$ . Clearly, this is an extreme example, and would require from an experimental point of view a “soft”, rubberlike material, with some sort of high-quality polymeric healing agent. However, numerical data indicate that the possibility exists, in agreement with previous results by the authors, showing that hierarchy alone is unable to provide

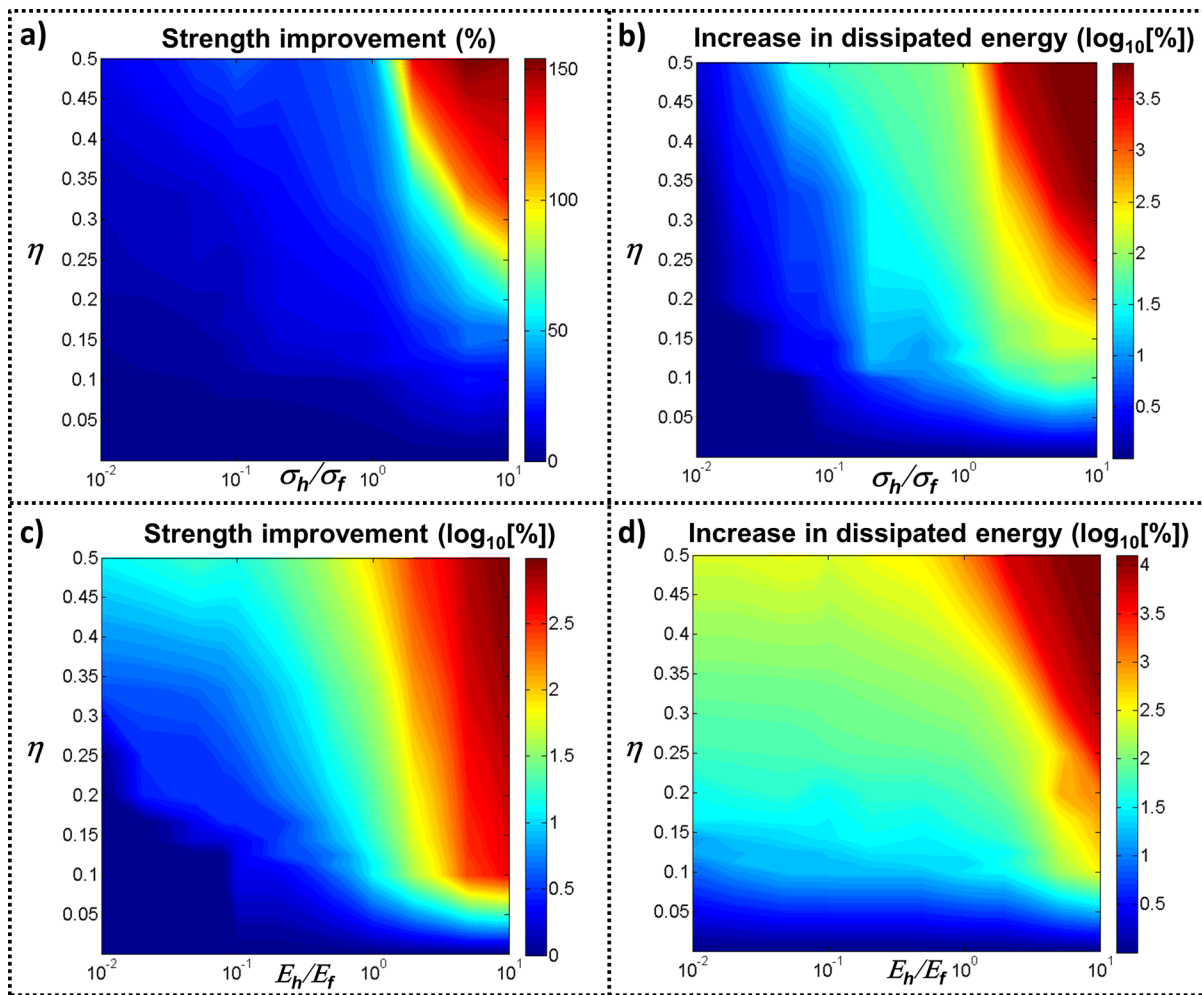


**Figure 7.** Maps showing percentage improvement in overall material properties as a function of healing rate  $\eta$  and host material vs healing agent properties: (a) Strength improvement for varying host material strength  $\sigma_f$  and healing agent strength  $\sigma_h$  ( $E_f = E_h$ ). (b) Increase in dissipated energy for varying  $\sigma_f$  and  $\sigma_h$  (log scale,  $E_f = E_h$ ). (c) Strength improvement for varying host material stiffness  $E_f$  and healing agent stiffness  $E_h$  (log scale,  $\sigma_f = \sigma_h$ ). (d) Increase in dissipated energy for varying  $E_f$  and  $E_h$  (log scale,  $\sigma_f = \sigma_h$ ). All results are for local SH.

improved mechanical properties, while hierarchy and material mixing is.<sup>27</sup>

If we now consider SH to occur only at one specific size scale or hierarchical level, the overall strengthening effect with respect to the non-SH case is reduced, as shown in Figure 9. Only results from numerical simulations are reported here, for simplicity. It is interesting to observe that the lower the hierarchical level at which SH occurs, the more effective the healing is, particularly for high  $\eta$  values. Indeed, there is only a small decrease in strength between the case in which SH takes place at all levels and the case in which it only occurs at the lowest hierarchical level. These results suggest that the most effective SH strategies could thus lie at microscopic or molecular level.

Next, we investigate the combined effect of SH and hierarchy on the strength of different hierarchical architectures. For simplicity, we consider four different hierarchical structures made up of  $N = 8$  fibers, differing only in hierarchical structure, which varies from one to three hierarchical levels. The first-level structure consists of eight parallel fibers (indicated as “(8,1)”). The properties of each of these level 1 fibers is derived from the level 0 Weibull statistics, including SH. There are two level 2 structures, indicated as “(4,2)”, that is, four bundles of two fibers in parallel and “(2,4)”, that is, two bundles of four fibers

in parallel. Finally, there is one level 3 structure indicated with “(2,2,2)”, that is, two bundles of two fiber bundles. These structures are schematically illustrated in Figure 10. Only analytical calculations are discussed here. If one considers SH to be present at all hierarchical levels, we find as above that the strength of all 4 structures (normalized with respect to the chosen Weibull scale parameter) increases with increasing SH parameter, as shown in Figure 10. What is interesting, however, is that the relative strength between the four structures is reversed as  $\eta$  increases: when no SH is present, the nonhierarchical structure (8,1) has the highest strength, while for  $\eta > 0.2$ , the third level structure (2,2,2) becomes the most favorable. Thus, the tendency found in previous publications for nonhierarchical structures<sup>28</sup> is reversed, and we find that hierarchy enhances the effect of SH. Moreover, these results point to the fact that in the presence of SH, the effect of hierarchy is to improve mechanical material characteristics. This tendency is precisely what is found in real biomaterials, where the ability of self-healing combines with a natural hierarchical structure to give enhanced structural properties. This finding is extremely important as it shows that the conflict between strength and hierarchy can be resolved by introducing self-healing as an additional design variable. This can provide

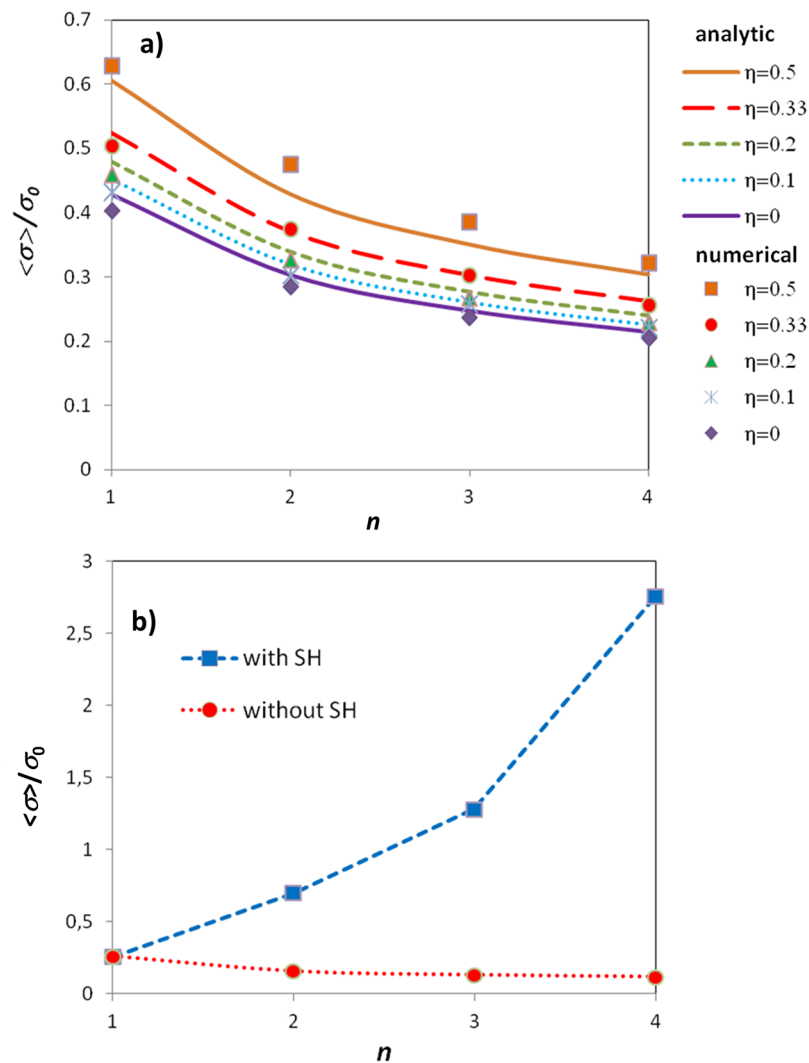


**Figure 8.** Scaling of the ratio between mean strength and Weibull scale parameter as a function of hierarchical level  $n$ : a) Comparison between analytical calculations and numerical simulations for various  $\eta$  values (distributed SH); b) Numerical comparison between “without SH” ( $\eta_1 = \eta_2 = \eta_3 = \eta_4 = 0$ ) and “with SH” ( $\eta_1 = 0, \eta_2 = 0.11, \eta_3 = 0.17, \eta_4 = 0.25$ ) when the healing agent mechanical properties are considerably superior to those of the host material (see text for details).

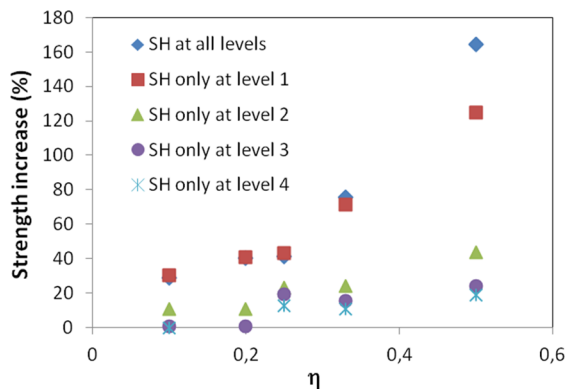


**Figure 9.** Strength increase with respect to the non-SH case in 4-level hierarchical structures as a function of  $\eta$  when SH is applied at a single or at all hierarchical levels.

inspiration for scientists and engineers to design multifunctional artificial materials with optimized properties.

## 5. CONCLUSIONS

We have presented numerical results on the mechanical behavior of self-healing hierarchical materials, using a previously developed Hierarchical Fiber Bundle Model. The model allows one to consider varying healing rates and different healing mechanisms, depending on where fibers are restored in the considered bundle. Results show that considerable improvements can be obtained in material strength and time to failure, and especially in material toughness. Simulations on hierarchical materials reveal the advantages of achieving self-healing at the smallest possible scale, and the possibility of inverting the strength scaling behavior (“smaller is stronger”) when using healing agents with appropriate mechanical properties. Finally, we show that combining self-healing and hierarchy begets superior strength, as observed in natural materials. These results are promising for further more in-depth investigations in the possibilities of self-repairing materials, and the presented analytical/numerical model can constitute a useful tool to support experimental work and aid in the attempt to synthesize real self-healing materials with tailor-made properties.

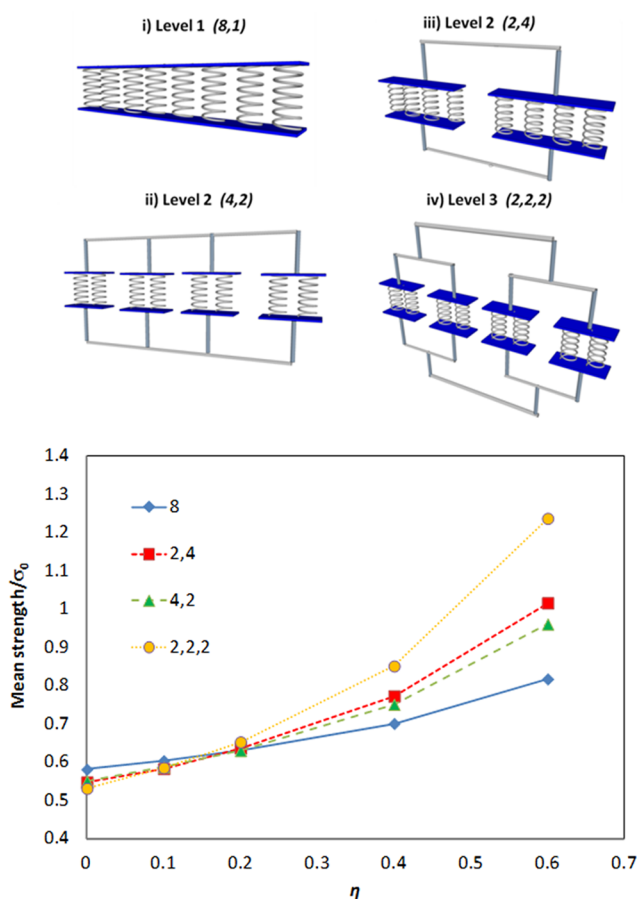


**Figure 10.** Schematic of different hierarchical fiber architectures, ranging from 1 level (i) to 3 hierarchical levels (iv), and their variation of normalized mean strength vs SH parameter. SH is shown to be more effective in the structure with highest hierarchy.

## AUTHOR INFORMATION

### Corresponding Author

\*E-mail: nicola.pugno@unitn.it.

### Notes

The authors declare no competing financial interest.

## ACKNOWLEDGMENTS

N.M.P. acknowledges support from the European Research Council, ERC Ideas Starting Grant No. 279985 “BIHSNAM: Bio-inspired Hierarchical Super Nanomaterials” and ERC Proof of Concept Grant No. 619448 “REPLICA2: Large-area replication of biological anti-adhesive nanosurfaces” and from the European Commission within the Graphene Flagship. F.B. acknowledges support from BIHSNAM. The authors thank F. Della Croce and the related support from the computational resources at Politecnico di Torino’s DAUIN High Performance Computing Initiative ([www.dauin-hpc.polito.it](http://www.dauin-hpc.polito.it)).

## REFERENCES

(1) White, S. R.; Sottos, N. R.; Geubelle, P. H.; Moore, J. S.; Kessler, M. R.; Sriram, S. R.; Brown, E. N.; Viswanathan, S. Autonomic healing of polymer composites. *Nature* **2001**, *409*, 794–797.  
 (2) Jones, A. S.; Rule, J. D.; Moore, J. S.; Sottos, N. R.; White, S. R. Life extension of self-healing polymers with rapidly growing fatigue cracks. *J. R. Soc. Interface* **2007**, *4*, 395–403.

(3) Chen, X. X.; Dam, M. A.; Ono, K.; Mal, A.; Shen, H. B.; Nutt, S. R.; Sheran, K.; Wudl, F. A thermally re-mendable cross-linked polymeric material. *Science* **2002**, *295*, 1698–1702.

(4) Toohey, K. S.; Sottos, N. R.; Lewis, J. A.; Moore, J. S.; White, S. R. Self-healing materials with microvascular networks. *Nat. Mater.* **2007**, *6*, 581–585.

(5) Hansen, C. J.; Wu, W.; Toohey, K. S.; Sottos, N. R.; White, S. R.; Lewis, J. A. Self-healing materials with interpenetrating microvascular networks. *Adv. Mater.* **2009**, *21*, 4143–4147.

(6) Brown, E. N.; White, S. R.; Sottos, N. R. Retardation and repair of fatigue cracks in a microcapsule toughened epoxy composite - Part II: In situ self-healing. *Compos. Sci. Technol.* **2005**, *65*, 2474–2480.

(7) Cordier, P.; Tournilhac, F.; Soulie-Ziakovic, C.; Leibler, L. Self-healing and thermoreversible rubber from supramolecular assembly. *Nature* **2008**, *451*, 977–980.

(8) Burnworth, M.; Tang, L. M.; Kumpfer, J. R.; Duncan, A. J.; Beyer, F. L.; Fiore, G. L.; Rowan, S. J.; Weder, C. Optically healable supramolecular polymers. *Nature* **2011**, *472*, 334–337.

(9) Chen, Y.; Kushner, A. M.; Williams, G. A.; Guan, Z. Multiphase design of autonomic self-healing thermoplastic elastomers. *Nat. Chem.* **2012**, *4*, 467–472.

(10) Murphy, E. B.; Wudl, F. The world of smart healable materials. *Prog. Polym. Sci.* **2010**, *35*, 223–251.

(11) Verberg, R.; Dale, A. T.; Kumar, P.; Alexeev, A.; Balazs, A. C. Healing substrates with mobile, particle-filled microcapsules: designing a ‘repair and go’ system. *J. R. Soc. Interface* **2007**, *4*, 349–357.

(12) Maiti, S.; Shankar, C.; Geubelle, P. H.; Keiffer, J. Continuum and molecular-level modeling of fatigue crack retardation in self-healing polymers. *J. Eng. Mater.-T. ASME* **2006**, *128* (4), 595–602.

(13) Salib, I. G.; Kolmakov, G. V.; Gnegy, C. N.; Matyjaszewski, K.; Balazs, A. C. Role of parallel reformable bonds in the self-healing of cross-linked nanogel particles. *Langmuir* **2011**, *27*, 3991–4003.

(14) Salib, I. G.; Kolmakov, G. V.; Bucior, B. J.; Peleg, O.; Kroger, M.; Savin, T.; Vogel, V.; Matyjaszewski, K.; Balazs, A. C. Using mesoscopic models to design strong and tough biomimetic polymer networks. *Langmuir* **2012**, *27*, 13796–13805.

(15) BaLazs, A. C. Modelling self-healing materials. *Mater. Today* **2007**, *10*, 18–23.

(16) Yuan, Q.; Xu, Z.; Yakobson, B. I.; Ding, F. Efficient defect healing in catalytic carbon nanotube growth. *Phys. Rev. Lett.* **2012**, *108*, 245505.

(17) Zan, R.; Ramasse, Q. M.; Bangert, U.; Novoselov, K. S. Graphene reknits its holes. *Nano Lett.* **2012**, *12*, 3936–3940.

(18) Shi, X.; Cheng, Y.; Pugno, N. M.; Gao, H. A translational nanoactuator based on carbon nanoscrolls on substrates. *Appl. Phys. Lett.* **2010**, *96*, 053115.

(19) Lakes, R. Materials with structural hierarchy. *Nature* **1993**, *361*, 511–515.

(20) Fratzl, P.; Weinkamer, R. Nature’s hierarchical materials. *Prog. Mater. Sci.* **2007**, *52*, 1263–1334.

(21) Currey, J. D. Hierarchies in biomineral structures. *Science* **2005**, *309*, 253–254.

(22) Qian, H.; Greenhalgh, E. S.; Shaffer, M. S. P.; Bismarck, A. Carbon nanotube-based hierarchical composites: a review. *J. Mater. Chem.* **2010**, *20*, 4751–4762.

(23) Daniels, H. E. The statistical theory of the strength of bundles of threads. *Proc. R. Soc. London, Ser. A* **1945**, *183*, 405–435.

(24) Pradhan, S.; Hansen, A.; Chakrabarti, B. K. Failure processes in elastic fiber bundles. *Rev. Mod. Phys.* **2010**, *82* (1), 499–555.

(25) Pugno, N.; Abdalrahman, T. Modeling the self-healing of biological or bio-inspired nanomaterials. *Int. Space Eleva. Consortium J., CLIMB* **2011**, *1*, 79–86.

(26) Weibull, W. A Statistical theory of the strength of materials. *Ingenioersvetenskapsakad., Handl.* **1939**, 151.

(27) Bosis, F.; Abdalrahman, T.; Pugno, N. M. Investigating the role of hierarchy on the strength of composite materials: evidence of a crucial synergy between hierarchy and material mixing. *Nanoscale* **2012**, *4*, 1200–1207.

(28) Pugno, N. M.; Bosia, F.; Abdalrahman, T. Hierarchical fiber bundle model to investigate the complex architectures of biological materials. *Phys. Rev. E* **2012**, *85*, 011903.

(29) Bosia, F.; Pugno, N.; Lacidogna, G.; Carpinteri, A. Mesoscopic modeling of acoustic emission through an energetic approach. *Int. J. Solids Struct.* **2008**, *45*, 5856–5866.

(30) Pugno, N. M.; Bosia, F.; Carpinteri, A. Multiscale stochastic simulations for tensile testing of nanotube-based macroscopic cables. *Small* **2008**, *4*, 1044–1052.

(31) Bosia, F.; Buehler, M. J.; Pugno, N. M. Hierarchical simulations for the design of supertough nanofibers inspired by spider silk. *Phys. Rev. E* **2010**, *82*, 056103.